2-15-2010

Tunneling between carbon nanofiber and gold electrodes

Toshishige Yamada
Santa Clara University, tyamada@scu.edu

Tsutomu Saito

Makoto Suzuki

Patrick Wilhite
Santa Clara University, pwilhite@scu.edu

Xuhui Sun

See next page for additional authors

Recommended Citation
T. Yamada, T. Saito, M. Suzuki, P. Wilhite, X. Sun, N. Akhavantafti, D. Fabris, and C.Y. Yang, "Tunneling between carbon nanofiber and gold electrodes," Journal of Applied Physics 107, 044304 (5 pp) (2010). https://doi.org/10.1063/1.3295901

Authors
Toshishige Yamada, Tsutomu Saito, Makoto Suzuki, Patrick Wilhite, Xuhui Sun, Navid Akhavantafti, Drazen Fabris, and Cary Y. Yang

Tunneling between carbon nanofiber and gold electrodes

Toshishige Yamada,[a] Tsutomu Saito,[b] Makoto Suzuki,[b] Patrick Wilhite, Xuhui Sun,[c] Navid Akhavantafti, Drazen Fabris, and Cary Y. Yang
Center for Nanostructures, Santa Clara University, 500 El Camino Real, Santa Clara, California 95053, USA

(Received 13 July 2009; accepted 26 December 2009; published online 18 February 2010)

In a carbon nanofiber (CNF)-metal system such as a bridge between two gold electrodes, passing high current (current stressing) reduces the total resistance of the system (CNF resistance R_{CNF} plus contact resistance R_c) by orders of magnitude. The role of current stressing is modeled as a reduction in the interfacial tunneling gap with transport characteristics attributed to tunneling between Au and CNF. The model predicts a reduction in R_c and gradual disappearance of the nonlinearity in the current-voltage (I-V) characteristics as R_c decreases. These results are consistent with measured I-V behavior. © *2010 American Institute of Physics*. [doi:10.1063/1.3295901]

I. INTRODUCTION

Carbon nanostructures such as carbon nanofibers (CNFs) are expected to play an important role in next-generation electronics, especially in interconnects due to immunity for electromigration.[1–7] CNF belongs to the graphene family and has cup-shaped stacked-cones in the interior and graphene-sheet outer walls similar to those in multiwall carbon nanotube (CNT),[8] with diameters ranging from 50 to 200 nm. Compared to CNTs, CNFs can be grown at lower temperature and easily aligned vertically, which is advantageous for via interconnect applications.[9] A four-point probe measurement revealed nearly linear current-voltage (I-V) behavior, suggesting that CNFs are metallic.[10] Because of their relatively large diameters compared with single-wall CNTs, one would not expect quantum confinement effects in CNFs and a resulting semiconducting phase with a finite bandgap at room temperature.[11] Here, we study structures where CNFs are simply placed on top of prefabricated Au electrodes, as a model for horizontal on-chip interconnects. In this Au-CNF-Au system, initial resistance is typically in the megaohm range but after conducting an appreciable amount of current (10^5–10^6 A/cm^2) for a few minutes, the resistance is reduced by two to three orders of magnitude. This process is called current stressing. Here, we present a tunneling model to analyze the measured I-V characteristics in each stage of current stressing and elucidate the resulting large resistance change. This is the first reported use of a tunneling model for explaining the current stressing effect in drop-cast contact.

II. CURRENT STRESSING EXPERIMENT

The present experiment uses CNFs grown with a plasma-enhanced chemical vapor deposition process and Ni catalyst on a SiO_2 substrate.[9] The nanofibers thus grown are dispersed in an isopropyl alcohol solution and drop-casted on patterned Au electrodes fabricated on an oxide-covered Si wafer.[12] An example of the resulting Au-CNF-Au structure is shown in the scanning electron microscope (SEM) image in Fig. 1(a).[13] The CNF shown is about 200 nm wide (diameter) and 4 μm long (including the segments on Au electrodes). In the current stressing experiment,[14] a large stress current is applied. Then, we measure the I-V characteristics using a much smaller current so that the system stays at room temperature. In the next cycle, a larger stress current is applied. The process is repeated until the CNF breaks down. The same experiment is performed for multiple samples and all

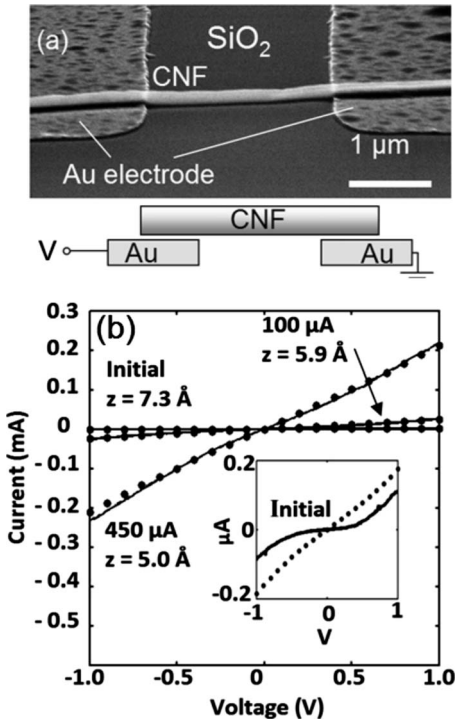

FIG. 1. (a) SEM image of a Au-CNF-Au system on SiO_2 substrate. (b) Measured I-V before and after multiple current stressing. Current stressing conditions are shown with current magnitude and duration time. Solid circles are modeling results at 300 K, with fitted z=7.3, 5.9, and 5.0 Å and measured S=0.125 μm^2 from SEM.

[a]Author to whom correspondence should be addressed. Electronic mail: tyamada@scu.edu.
[b]Present address: Hitach High-Technologies Corp., Japan.
[c]Present address: FUNSOM, Soochow University, People's Republic of China.

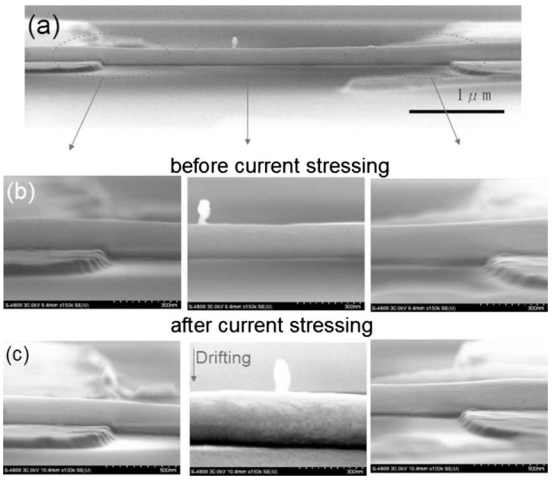

FIG. 2. SEM image of a Au-CNF-Au system before and after current stressing.

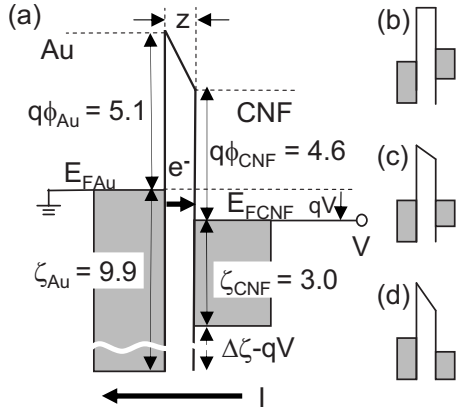

FIG. 3. Energy band model between the Au and CNF with a vacuum tunneling gap of width z. CNF is biased at V with respect to grounded Au, where current per unit area J flows from CNF to Au. $q\phi$ is work function, ζ is Fermi level depth measured from the bottom of the band, and E_F is Fermi level position. $\Delta\zeta=\zeta_{FAu}-\zeta_{FCNF}$ is the difference between the Fermi level depths. The energy band is shown for CNF bias at (b) $V<0$, (c) $V=0$, and (d) $V>0$.

display a very similar behavior.[14] Figure 1(b) shows three *I-V* curves for one of these samples, at the initial state, after going through current stressing cycles up to 100 μA, and after cycles up to 450 μA (Ref. 15) (solid circles are modeling results to be discussed later). The resistance decreases by two orders of magnitude for current stressing cycles up to 100 μA, while by only an order of magnitude or less from 100 μA to 450 μA. The improvement by current stressing does not continue indefinitely. This result is observed for all samples.

In Fig. 2, SEM images before and after current stressing are shown. From these images, there is no evidence for any significant change in the contact geometry or bulk CNF, although the total resistance between the two electrodes R_{tot} decreases by orders of magnitude. In the current stressing experiment, Saito *et al.*[13] compared two different kinds of electrode contacts, drop-cast as used here versus tungsten-deposited, where the deposited W wraps around the CNF, increasing the contact area significantly. In the drop-cast samples, the initial R_{tot} was on the order of magaohms but after progressive current stressing, it was reduced to the kilohm range, as shown in Fig. 1(b). In the W-deposited electrode samples, R_{tot} was practically unchanged and stays in the kilohm range at room temperature, even though the CNF must have been heated up significantly during each stress cycle. The largest change in R_{tot} for these samples was at most 20%. This sharp contrast between the two different contacts strongly suggests that current stressing changes primarily the electrode contacts and not the CNF bulk. We have also performed four-point probe measurements and the average resistivity for *unstressed* CNF is $\rho_{CNF}=1.3\times10^{-5}$ Ω m, which is in the same range as the result previously reported, 4.2×10^{-5} Ω m.[10] Using diameter $d\sim200$ nm and length $L\sim4$ μm, we obtain a CNF resistance $R_{CNF}=\rho_{CNF}\times L/\pi(d/2)^2=1.6$ kΩ, significantly lower than the measured R_{tot} in the MΩ range in Fig. 1(b), except for the very final stages before breakdown.

Thus, the substantial decrease in $R_{tot}=R_{CNF}+R_c$ from current stressing must be due to contact resistance R_c reduction, which can be attributed to physical changes in the nanostructure at the CNF-Au contacts. Thus, we propose that an interfacial region or gap with separation z exists at each electrode contact and electrons tunnel across it. After drop-cast, the initial interfacial geometry is expected to be rough due to weak attractive forces between CNF and Au. Current stressing supplies Joule heat to the materials, equivalent to thermal annealing, resulting in improved interfacial geometry and an effective decrease in z. This is the primary premise of our model in describing the role of current stressing in total resistance reduction.

III. TUNNELING MODEL

We now examine the tunneling transport between Au and CNF. These are two different metals having different work functions and Fermi level depth. The band structure is shown in Fig. 3(a). Au has a work function $q\phi_{Au}$ of 5.1 eV (Ref. 16) and a Fermi level depth ζ_{FAu} of 9.9 eV (measured from the bottom of the band),[17] while CNF has a work function $q\phi_{CNF}$ of 4.6 eV and a Fermi level depth ζ_{FCNF} of 3.0 eV estimated using tight-binding theory.[18] $\Delta\zeta=\zeta_{FAu}-\zeta_{FCNF}=6.9$ eV is the difference between the Fermi level depths. The tunneling probability P_t is independent of the tunneling direction. The tunneling barrier with width z models the interfacial region. The energy bands for different biases are $V<0$, $V=0$, and $V>0$ [shown in Figs. 3(b)–3(d)]. Using the bias V with respect to Au, we obtain $E_{F1}=E_{F2}+qV$.

In the tunneling process, the total energy is undoubtedly conserved, but the momentum parallel to the vacuum gap may or may not be, depending on the junction surfaces. When the Au and CNF surfaces are smooth enough so that there is no horizontal force for an electron during tunneling, it will be conserved.[19] When the surfaces are rough, the momentum will not be conserved.[20] Therefore, we derive two formulas corresponding to these cases. The detailed derivation, including the form of P_t and the conditions of small voltage swing with an assumption of $m_1\sim m_2$, is given in the Appendix.

When parallel momentum is conserved, we obtain

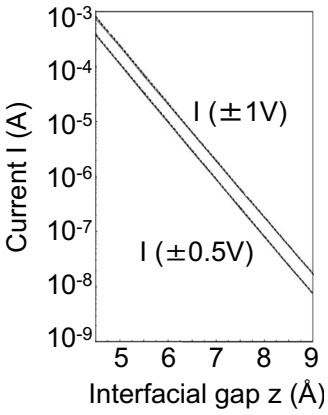

FIG. 4. Current I at ± 1 and ± 0.5 V as a function of interfacial gap z at 300 K with $S=0.125\ \mu m^2$. Negative biases are shown with solid lines and positive biases are shown with broken lines, which virtually overlap.

$$J(k_{\|}cons) = \frac{qm_1}{2\pi^2\hbar^3}\int_{\Delta\zeta-qV}^{\infty} dE[f(E,E_{F1}) - f(E,E_{F1}-qV)] \times \int_{\Delta\zeta-qV}^{E} dW_1 P_t(W_1), \quad (1)$$

When parallel momentum is not conserved, we obtain

$$J(k_{\|}ncons) = \frac{qm_1}{2\pi^2\hbar^3}\int_{\Delta\zeta-qV}^{\infty} dE[f(E,E_{F1}) - f(E,E_{F1}-qV)] \times \int_{0}^{E} dW_1 P_t(W_1). \quad (2)$$

The difference appears in the range of W integration. Equations (1) and (2) can be used in the general conditions for two different metals at any temperature. Both reduce to the well-known result by Simmons[21] for tunneling between two identical metals at low temperature.

In our Au-CNF system with a bias voltage magnitude of less than 1 V, there is no numerical difference between Eqs. (1) and (2). This is because Au and CNF work functions are quite deep (several eV) so that the tunneling probability $P_t(W)$ is negligibly small when $0 < W_1 < \Delta\zeta$. Thus, parallel momentum conservation will not significantly influence the results for this system, and all calculations here are performed using Eq. (1).

IV. COMPARISON OF MODEL WITH EXPERIMENT

In comparison of the present model to measured results, it is necessary to examine the meaning of the measured voltage. When the interface is smooth and charge/polarization-free (effective z is small), the measured voltage will be close to the difference $(E_{F1}-E_{F2})/q$. However, when z is large and there are charged or polarized impurities present in the interfacial region, there will be a voltage shift in the measured I-V curve from that predicted by tunneling theory.[22] Thus, we compare dI/dV with its experimental counterparts rather than I itself for prestressed devices. Such situations are also found in other systems,[22,23] possibly due to similar mechanisms in the interfacial region.

Figure 4 shows calculated current I as a function of interfacial gap z at $V=\pm 0.5$ and ± 1 V for a *single* Au-CNF junction at 300 K, where CNF is biased at V with respect to Au. Negative bias cases are shown with solid lines and positive bias cases with broken lines. Au-CNF contact area $S=0.125\ \mu m^2$ is measured from the SEM image in Fig. 1(a) and used throughout the calculation. I depends exponentially on z and increases by an order of magnitude for either curve in Fig. 4 as z decreases by ~ 1 Å. Such strong z dependence is characteristic of tunneling transport.

When *two* Au-CNF tunneling junctions 1 and 2 with z_i and S_i $(i=1,2)$ are connected in series as in Fig. 1(a), the junction with the larger z_i determines the total I-V characteristics. In the present CNF drop-cast method, the initial difference in z_i and S_i between two junctions is unavoidable, which infers that the difference of 10%–20% is quite common for S as seen in SEM images, and similar difference would be quite possible for z. Since the current depends exponentially on z as seen in Fig. 4, the junction with the larger z has much larger tunneling resistance than the other, resulting in the former junction dominating the total I-V characteristics. This is also the case for CNT tunneling junctions or Schottky junctions.[23,24]

We now apply the single-junction model to the circuit in Fig. 1(a). The current I is calculated at 300 K using $I=JS$, where $S=0.125\ \mu m^2$ as before, and z is the only adjustable parameter. The initial experimental I-V curve has clear asymmetry (if two junctions were identical, the I-V curve would be symmetric and the single-junction model can no longer apply). Charged and/or polarized residue in the interfacial region discussed above could be responsible as well as the intrinsically asymmetric Au-CNF tunneling junction. Modeling results (points) are compared with measured I-V curves (solid lines) at three different current stressing stages in Fig. 1(b). The prestressed I-V is fitted with $z=7.3$ Å. I-V curves after 100 and 450 μA current stressing cycles correspond to $z=5.9$ and 5.0 Å, respectively. As discussed above, dI/dV is used for fitting for $z=7.3$ Å of the prestressed case, and I for others. The nonlinearity in measured I-V curves tends to be smaller as R_{tot} decreases after current stressing, and the same trend is observed in our tunneling model. Since the CNF diameter (~ 100 nm) is much larger than that of the single-wall CNT (approximately several nanometers), the CNF-electrode contact surface is much larger as well as effectively flatter. Thus, the CNF-electrode contact area S is larger and the CNF-electrode separation z tends to be narrower compared with their CNT counterparts, resulting in a lower tunneling resistance.[5,25]

According to our model, current stressing reduces z of the dominant junction. Generally, van der Waals type interactions are common for neutral materials including graphitic structures, and are attractive at longer distances and repulsive at short distances with the equilibrium distance somewhere in between. These interactions allow CNFs to remain in place but are also responsible for attracting impurities into the system, adsorbed onto the graphitic sidewalls and electrode surfaces, which forms the interfacial region. Thus, the initial z tends to be larger than the equilibrium value. When the stress current is applied, Joule heat is generated at the Au-CNF interface. The temperature at contacts is expected to

be elevated above ambient during current stressing. Residues at the interface disappear through evaporation, oxidation, and/or chemisorption, leading to smaller z. The final z value is 5.0 Å. This gap distance is similar to another calculated distance between the nanotube and scanning tunnel microscope tip.[23] Once this z is reached, the van der Waals force will be approaching repulsive and no further reduction is expected. This is consistent with our observation that contact improvement by current stressing does not continue indefinitely.

Despite the expected increase in temperature due to Joule heating, we have not observed morphological changes in the contact geometry. R_{CNF} remains in the kΩ range throughout the stress cycles, while R_c is apparently reduced by a few orders of magnitude, from approximately megawatts to approximately kilowatts. When the stress current increases from 1 to 100 μA, R_c changes from approximately megawatts to ~10 kΩ and Joule heating power at the contact changes from approximately microwatts to ~0.1 mW, while that for the CNF bulk changes from approximately nanowatts to ~0.01 mW. Thus, the heating at the contacts is consistently dominant when the stress current is less than 100 μA. Indeed the Joule heating power is small, but heat generation is strongly localized at the contacts. This will bring about an increase in temperature and changes in the interface nanostructure at the contacts, corresponding to the observed two orders of change in R_{tot} shown in Fig. 1(b). When the stress current is further increased to several hundred microamperes, R_c is in the kilohm range, comparable to R_{CNF}, and Joule heat generation occurs fairly uniformly over the entire CNF. Assuming uniform heat generation throughout the entire system, one-dimensional heat transport consideration predicts that the generated Joule heat diffuses toward the electrodes and is dissipated there, resulting in the highest temperature at the midpoint of the CNF between the electrodes and close to ambient temperature at the contacts.[26] This is consistent with the observation that the resistance improvement does not last indefinitely. When the highest temperature exceeds the CNF threshold temperature [~900 K (Ref. 27)], breakdown occurs. When the stress current is less than ~100 μA, $R_c \gg R_{CNF}$ and primarily the contacts are modified due to Joule heating, but when the current is increased to several hundred microamperes, $R_c \sim R_{CNF}$ and the mid-point of the CNF experiences the maximum temperature, resulting in breakdown. Then, while it is highly unlikely that the Au melting temperature of ~1300 K is reached at the contacts during current stressing, the heat dissipated there is likely to result in nanoscale changes in the CNF-Au interface as described by our tunneling model, similar to what one would expect from thermal annealing.

The present findings generally apply to CNF interconnect systems without chemical bond formation between CNF and electrodes. In practical applications, more intimate and robust contacts must be fabricated (such as W-deposited electrodes in Ref. 13), and CNF bulk quality must also improve. However, R_c might still dominate the total system resistance. Since tunneling transport determines R_c, it is possible to improve the total system performance by making a more intimate contact (thus reducing the barrier width) or by placing charged and/or electrically polarized impurities intentionally in the interfacial region so that the CNF-electrode work function difference is decreased (reducing the barrier height).

V. CONCLUSION

Electron transport properties of a CNF bridging two Au electrodes, one of the simplest interconnect test structures, are studied and compared with single-junction tunneling model results. The model explains the key features of the measured I-V data, including improvement in linearity and decrease in resistance. The effect of current stressing is to reduce the tunneling gap, through change in interfacial nanostructure morphology and impurity reduction as a result of Joule heating.

ACKNOWLEDGMENTS

This work was supported by the United States Army Space and Missile Defense Command (SMDC) and carries Distribution Statement A, approved for public release, distribution unlimited.

APPENDIX: DERIVATION OF TWO TUNNELING CURRENT FORMULAS

We derive two tunneling current formulas with and without parallel momentum conservation. In the energy band diagram in Fig. 3(a), a relation $E_{F1}=E_{F2}+qV$ holds. The total energy E is conserved before and after tunneling. Thus,

$$\frac{\hbar^2}{2m_1}(k_{\parallel 1}^2+k_{\perp 1}^2)=\frac{\hbar^2}{2m_2}(k_{\parallel 2}^2+k_{\perp 2}^2)+\Delta\zeta-qV\equiv E. \quad \text{(A1)}$$

If parallel momentum is further conserved,

$$k_{\parallel 1}^2=k_{\parallel 2}^2\equiv k_{\parallel}^2\equiv\frac{2m_1E_{\parallel 1}}{\hbar^2}. \quad \text{(A2)}$$

$k_{\parallel i}$ ($k_{\perp i}$) is a parallel (perpendicular) wave vector in side i. m_i is the electron mass in side i. $\Delta\zeta=\zeta_{FAu}-\zeta_{FCNF}=6.9$ eV is the difference between the Fermi level depths and we consider a small voltage swing such that $\Delta\zeta>|qV|$ and the d-band in Au does not matter.[17] The tunneling probability P_t is independent of the tunneling direction. Using the Fermi–Dirac function $f_l=f(E,E_{Fl})=1/\{1+\exp[(E-E_{Fl})/k_BT]\}$ with $l=i,j$, the tunneling current density J from i to j is given by

$$\begin{aligned}J_{j\leftarrow i}&=q\sum_{\vec{k},spin}n(\vec{k})v_\perp(\vec{k})P_t f_i(1-f_j)\\&=\frac{2q}{(2\pi)^3}\int d(\pi k_\parallel^2)dk_\perp\frac{dE}{\hbar dk_\perp}P_t f_i(1-f_j)\\&=\frac{q}{4\pi^2\hbar}\int d(k_\parallel^2)dE P_t f(E,E_{Fi})[1-f(E,E_{Fj})].\end{aligned} \quad \text{(A3)}$$

Here n is the electron density, k_B is the Boltzmann constant, and T is the temperature. P_t is a function of the normal energy component $W_1=E-E_{\parallel 1}$, and is expressed with the Wentzel–Kramers–Brillouin approximation.[19] The energy barrier is expressed by $\Phi(z)=az+b$ with $a=(q\phi_2-q\phi_1$

$-qV)/z<0$ for a small swing and $b=q\phi_1>0$. The imaginary wave number $\kappa_\perp(z)$ of an electron is given by $\sqrt{2m_1(\Phi(z)-W)/\hbar}$, and

$$P_t(W_1)=\exp\left[-2\int \kappa_\perp(z)dz\right]=\exp\left\{-\frac{4}{3a}\sqrt{\frac{2m_1}{\hbar^2}}\times[(az+b-W_1)^{3/2}-(b-W_1)^{3/2}]\right\}, \quad \text{(A4)}$$

where the argument of the exponential function is negative. We assume $m_2\sim m_1$ and then calculate $J=J_{2\leftarrow1}-J_{1\leftarrow2}$. Whether the parallel momentum conservation of Eq. (A2) is present or not is reflected in the W_1 integration domain. When conserved, the smallest possible W_1 is $\Delta\zeta-qV$, and W_1 changes from $\Delta\zeta-qV$ to E. When not conserved, W_1 can take a value of 0, and W_1 changes from 0 to E. The domain of E integration is determined by the energy conservation in Eq. (A1), and E changes from $\Delta\zeta-qV$ to a very large value (still smaller than the minimum of $\Phi(z)$ but practically ∞) in both cases. Thus, we have the following:

When parallel momentum is conserved,

$$J(k_\parallel cons)=\frac{qm_1}{2\pi^2\hbar^3}\int_{\Delta\zeta-qV}^{\infty}dE[f(E,E_{F1})-f(E,E_{F1}-qV)]\times\int_{\Delta\zeta-qV}^{E}dW_1P_t(W_1), \quad \text{(A5)}$$

When parallel momentum is not conserved,

$$J(k_\parallel ncons)=\frac{qm_1}{2\pi^2\hbar^3}\int_{\Delta\zeta-qV}^{\infty}dE[f(E,E_{F1})-f(E,E_{F1}-qV)]\times\int_{0}^{E}dW_1P_t(W_1). \quad \text{(A6)}$$

[1] M. Nihei, A. Kawabata, D. Kondo, M. Horibe, S. Sato, and Y. Awano, Jpn. J. Appl. Phys., Part 1 **44**, 1626 (2005).
[2] S. Salahuddin, M. S. Lundstrom, and S. Datta, IEEE Trans. Electron Devices **52**, 1734 (2005).
[3] J. J. Plombon, K. P. O'Brien, F. Gstrein, V. M. Dubin, and J. Jiao, Appl. Phys. Lett. **90**, 063106 (2007).
[4] L. Dong, S. Youkey, J. Bush, J. Jiao, V. M. Dubin, and R. V. Chebiam, J. Appl. Phys. **101**, 024320 (2007).
[5] L. Fourdrinier, H. L. Poche, N. Chevalier, D. Mariolle, and E. Rouviere, J. Appl. Phys. **104**, 114305 (2008).
[6] J. O. Lee, C. Park, J. J. Kim, J. Kim, J. W. Park, and K. H. Yoo, J. Phys. D **33**, 1953 (2000).
[7] E. Minoux, O. Groening, K. B. K. Teo, S. H. Dalal, L. Gangloff, J. P. Shnell, I. Y. Y. Bu, P. Vincent, P. Legagneux, G. A. J. Amaratunga, and W. I. Milne, Nano Lett. **5**, 2135 (2005).
[8] V. I. Merkulov, M. A. Guillorn, D. H. Lowndes, M. L. Simpson, and E. Voelkl, Appl. Phys. Lett. **79**, 1178 (2001).
[9] Q. Ngo, A. M. Cassell, A. J. Austin, J. Li, S. Krishnan, M. Meyyappan, and C. Y. Yang, IEEE Electron Device Lett. **27**, 622 (2006).
[10] L. Zhang, D. Austin, V. I. Merkulov, A. V. Meleshko, K. L. Klein, M. A. Guillorn, D. H. Lowndes, and M. L. Simpson, Appl. Phys. Lett. **84**, 3972 (2004).
[11] M. S. Dresselhaus and M. Endo, in *Carbon Nanotubes: Synthesis, Structure, Properties, and Applications*, edited by R. E. Smalley, M. S. Dresselhaus, G. Dresselhaus, and Ph. Avouris (Springer, Boston, 2001).
[12] Y. Ominami, Q. Ngo, A. J. Austin, H. Yoong, C. Y. Yang, A. M. Cassell, B. A. Cruden, J. Li, and M. Meyyappan, Appl. Phys. Lett. **87**, 233105 (2005).
[13] T. Saito, T. Yamada, D. Fabris, H. Kitsuki, P. Wilhite, M. Suzuki, and C. Y. Yang, Appl. Phys. Lett. **93**, 102108 (2008).
[14] The initial resistance was significantly different from sample to sample, ranging from ~100 kΩ to ~10 MΩ as shown in Fig. 4 of Ref. 13. After progressive current-stressing cycles, the final resistance dropped and varied less among samples, ranging from ~3 kΩ to ~30 kΩ. The initial larger range is mainly due to R_c through variations in electrode-CNF contact area and in electrode-CNF separation (since $R_c \gg R_{CNF}$), while the smaller deviation after current stressing is due to both R_c and R_{CNF} through variations in CNF diameter and length, since $R_c \sim R_{CNF}$ as discussed later.
[15] The stress current is applied progressively as in Fig. 2(a) of H. Kitsuki, T. Yamada, D. Fabris, J. R. Jameson, P. Wilhite, M. Suzuki, and C. Y. Yang, Appl. Phys. Lett. **92**, 173110 (2008) (and 100 μA and 450 μA are representative of multiple current stressing cycles).
[16] *CRC Handbook of Chemistry and Physics*, edited by D. R. Lide (CRC, Boca Raton, 1998).
[17] N. E. Christensen, Phys. Rev. B **13**, 2698 (1976)), (the gold bandwidth is 9.9 eV determined by the *s*-band (one state). The *d*-band (five states) has a bandwidth of 5.8 eV and its top is 1.6 eV below the Fermi level).
[18] W. A. Harrison, *Electronic Structures and Properties of Solids* (Freeman, San Francisco, 1980).
[19] C. Duke, in *Tunneling in Solids, Solid State Physics, Suppl. 10*, edited by F. Seitz and D. Turnbull (Academic, New York, 1969).
[20] A. Bachtold, M. Henny, C. Terrier, C. Schönenberger, J. P. Salvetat, J. M. Bonard, and L. Forró, Appl. Phys. Lett. **73**, 274 (1998).
[21] J. G. Simmons, J. Appl. Phys. **34**, 1793 (1963).
[22] T. Yamada, Appl. Phys. Lett. **88**, 083106 (2006).
[23] T. Yamada, Appl. Phys. Lett. **78**, 1739 (2001).
[24] T. Yamada, Appl. Phys. Lett. **80**, 4027 (2002).
[25] Z. Yao, C. L. Kane, and C. Dekker, Phys. Rev. Lett. **84**, 2941 (2000).
[26] T. Yamada, T. Saito, D. Fabris, and C. Y. Yang, IEEE Electron Device Lett. **30**, 469 (2009).
[27] K. Hata, D. N. Futaba, K. Mizuno, T. Namai, M. Yumura, and S. Iijima, Science **306**, 1362 (2004).